Evolution of dispersoids during multistep heat treatments and their effect on rolling performance in an Al-5% Mg-0.8% Mn alloy

Ahmed Y. Algendy, Kun Liu*, X.-Grant Chen
Department of Applied Science, University of Quebec at Chicoutimi, Saguenay (QC), G7H 2B1, Canada

*Corresponding author: kun.liu@uqac.ca; Tel.: 01-4185455011 ext. 7112; Fax: 01-4185455012

Abstract

The precipitation behavior of dispersoids in an Al-5% Mg-0.8% Mn alloy after various single-and multistep heat treatments and their effect on rolling performance were investigated. The results show a significant increase in the electrical conductivity and microhardness caused by the precipitation of submicron dispersoids after all heat treatments. In addition, the multistep heat treatments resulted in higher microhardness and a larger fraction of dispersoid zones than single-step treatments. Two types of Mn-bearing dispersoids with cube- and rod-like morphologies were identified. The low-temperature two-step heat treatment (275 °C/12 h + 375 °C /48 h) produced the highest number density of dispersoids with the finest size among all the studied heat treatments but severe defects were created during hot-rolling. The three-step heat treatment (275 °C/12 h + 375 °C/48 h + 500 °C/4 h) provided the best combination of dispersoid characteristics and rolling performance. The mechanical properties of rolled sheets subjected to the three-step heat treatment were improved compared to those treated using industrial homogenization treatment, owing to the higher number density and finer size of the dispersoids.

Keywords: Al-Mg-Mn alloy, Dispersoids, Multi-step heat treatment, Microstructure, Rolling performance, Mechanical properties

1. Introduction

Owing to their attractive combination of high strength, good formability, weldability, and excellent corrosion resistance, Al-Mg-Mn alloys are widely used in the automotive industry and in marine applications [1, 2]. Unlike heat-treatable alloys such as 2xxx, 6xxx, and 7xxx, Al-Mg 5xxx alloys derive their strength mainly from work hardening and solid solution strengthening due to Mg, which has substantial solid solubility in aluminum [3, 4]. Currently, considerable efforts are being made to improve the mechanical properties of aluminum alloys, which can help achieve weight reduction in automotive and aerospace applications. In recent years, dispersion strengthening has attracted considerable attention as a promising avenue for improving the mechanical properties of non-heat-treatable aluminum alloys [5–8]. Several studies have demonstrated that precipitation of fine, thermally stable dispersoids using appropriate heat treatments can be an effective way to enhance the room- and elevated-temperature properties of aluminum alloys, such as in 3xxx wrought alloys [7, 9, 10]. The dispersoid strengthening effect is strongly dependent

on their type, size, volume fraction, and distribution, which are in turn related to the alloy chemistry and heat treatment conditions [6, 7, 11, 12].

In Al-Mg-Mn 5xxx alloys, it has long been recognized that the precipitation of submicron dispersoids plays an important role in recrystallization resistance during the hot deformation process by retarding both the movement of dislocations and grain boundary migration [5, 13, 14]. Ratchev *et al.* [15] reported that two different morphologies of $Al_6(Mn,Fe)$ dispersoids with high and low aspect ratios occurred in AA5182 alloy at different preheating temperatures during homogenization. Engler *et al.* [14, 16, 17] found that two major types of dispersoids $Al_6(Mn,Fe)$ and α-Al(Fe,Mn)Si, could precipitate in 5xxx alloys and that the type of dispersoids was strongly controlled by the Mg and Si contents. In other studies [18, 19], it was found that Cr-bearing dispersoids could be formed during homogenization at relatively low temperatures, which were identified as ν-$Al_{18}(Cr,Mn)_2Mg_3$. In general, the contribution of these dispersoids to improving the mechanical properties is rather limited owing to their large size and low volume fraction.

Many efforts have been made in Al-Mg-Mn 5xxx alloys to study the precipitation of dispersoids at relatively high temperatures because 5xxx alloys are generally subjected to conventional high-temperature homogenization (500–550 °C) prior to hot rolling. However, homogenization treatment at high temperature resulted in the precipitation of only a few coarse dispersoids, which showed little strengthening effect [17, 18].Therefore, it is necessary to significantly decrease the size of the dispersoids and increase their volume fraction to improve the mechanical properties of 5xxx alloys. Recent studies on 3xxx and 6xxx alloys indicated that heat treatment at relatively low temperatures (i.e., 350–450 °C) could promote dispersoid precipitation and produce a large volume fraction of finer dispersoids [7, 8, 20]. However, limited information in the literature has been found on how to improve the precipitation of dispersoids through heat treatment in 5xxx alloys.

The present study was undertaken to investigate the evolution of dispersoids in a typical as-cast Al-5% Mg-0.8% Mn alloy alloy after a broad range of heat treatments. Several characterization techniques, including optical microscopy, scanning electron microscopy with energy dispersive X-ray spectrometry, transmission electron microscopy, electrical conductivity, and microhardness measurements were used to characterize the as-cast and heat-treated microstructures. The rolling performance and tensile properties of the rolled sheets after various heat treatments were also evaluated.

2. Experimental procedures

The experimental Al-5% Mg-0.8% Mn alloy was prepared by batching commercially pure Al (99.7 wt.%), pure Mg (99.9 wt.%), Al-25% Fe, Al-50% Si, Al-25%Mn, Al-50%Cu and Al-20% Cr master alloys. The chemical composition of the experimental alloy, which is close to AA5083 and AA5183 alloys, was analyzed using an optical emission spectrometer, and the result is shown in Table 1. Approximately 3 kg of the material was melted in a graphite crucible using an electrical resistance furnace. The melt temperature was maintained at 780 °C for 30 min, followed by Ar-degassing for 15 min. The melt was then grain-refined using Al-5% Ti-1% B master alloy and finally poured into a preheated steel mold at 250 °C. The dimensions of the cast ingots were 30 mm × 40 mm× 80 mm.

Table 1 Chemical composition of experimental alloy (wt.%)

Mg	Mn	Si	Fe	Cu	Cr	Ti	Al
5.23	0.78	0.26	0.31	0.11	0.18	0.11	Bal.

To study the precipitation behavior of the dispersoids, the as-cast ingots were heat-treated at different temperatures for various time periods, followed by water quenching; the details of the procedures are shown in Table 2. The first three single-step treatments were used to examine the precipitation behavior of the dispersoids at different temperatures. Multistep heat treatments (2S-LT, 2S-HT, and 3S-LT54) were designed not only to further optimize the dispersoid characteristics (size, number density, and distribution), but also to adapt to the rolling process. The last treatment (I-Homo) represents a common industrial homogenization practice for Al-Mg-Mn 5xxx alloys prior to hot rolling [21]. The heat treatments were conducted in a programmable electrical air circulating furnace at a heating rate of 60 °C /h. Subsequently, the ingots were hot-rolled using a lab-scale rolling unit in the temperature range of 460–500 °C. When the temperature of the rolled strip fell below 460 °C, the strip was placed back in the furnace to reheat to 500 °C between the rolling passes. After multiple passes, the block was reduced to a final sheet thickness of 3.2 mm with an area reduction of 88%. All rolled sheets were further annealed at 300 °C for 5 h to relieve the rolling-induced thermal stress prior to tensile testing.

Table 2 Heat treatments applied in experimental alloy

Code	Parameters
SS3	375 ^{o}C/6, 12, 24, 48 h
SS4	425 ^{o}C/2, 6, 12, 24 h
SS5	500 ^{o}C/2, 6, 12, 24 h
2S-LT	275 ^{o}C/12 h + 375 ^{o}C/48 h
2S-HT	425 ^{o}C/24 h + 500 ^{o}C /4 h
3S-LT54	275 ^{o}C/12 h + 375 ^{o}C/48 h + 500 ^{o}C/4 h
I-Homo	430 ^{o}C/2 h + 480 ^{o}C/2 h + 525 ^{o}C/2 h

The grain structure was characterized under polarized-light optical microscopy after electro-etching using Barker's reagent (3 vol.% HBF4 solution) at 15 V for 3 min. The average grain size was measured using the linear intercept method according to ASTM E112-12 on electro-etched samples in optical microscopy with polarized light. At least 10 fields containing ~ 500 grains each under 50X were analyzed. To observe the dispersoid zones (DZs) and dispersoid-free zones (DFZs), the heat-treated samples were etched in 0.5% HF for 35 s. Image analysis with Clemex PE 4.0 software was used to measure the DZ and DFZ area fractions as well as the area fraction of various intermetallic particles. More than 50 fields were randomly chosen and analyzed, and the average area fraction of intermetallic particles was calculated with those measurements. A scanning electron microscope (SEM, JSM-6480LV) equipped with an energy-dispersive X-ray spectrometer (EDS) was used to

identify the composition of the intermetallics. To reveal the details of the dispersoids, a transmission electron microscope (TEM, JEM-2100) operating at 200 kV was used. TEM foils were prepared in a twin-jet electro-polisher using a solution of 30% HNO_3 in methanol at a temperature of −20 °C. The thickness of the observed area in the TEM was measured using convergent electron beam diffraction. All TEM images were taken along the $[001]_{Al}$ zone axis. The size and number density of the dispersoids were measured using image analysis software (ImageJ) on the TEM images. The number density of the dispersoids was determined using the following equation:

$$ND = \frac{N}{A*(D+t)} \quad (1)$$

where N is the number of particles in the TEM image, A is the total area, D is the equivalent diameter, and t is the thickness of the TEM foil, which was measured using convergent electron beam diffraction (CBED) method [22].

The precipitation behavior of dispersoids was also evaluated through electrical conductivity measurements using a Sigmascope SMP 10 device at room temperature. Vickers microhardness was determined both after heat treatment and after rolling using an NG-1000 CCD machine with a 25-g load and a 20-s dwell time. Twenty measurements were performed to determine the average value of each sample. To evaluate the mechanical properties after hot rolling, tensile tests at room temperature were conducted using an Instron 8801 servo-hydraulic unit at a strain rate 0.5 mm/min. The tensile sheet samples were machined according to ASTM E8/E8M-16A in the rolling direction with a gauge area of 3 × 10 mm.

3. Results and discussion

3.1 As-cast to heat-treated microstructural evolution

Fig. 1 shows the grain structure and evolution of the intermetallic particles from the as-cast condition through heat treatment. The as-cast grain structure of the experimental alloy was characterized as equiaxed grains with an average size of 63.8 ± 7.7 μm (Fig. 1a). At a higher magnification (Fig. 1b), the microstructure is composed of aluminum dendrite cells surrounded by a number of different intermetallics, which were discussed in detail in our previous work [23]. In brief, the dominant intermetallic phases are Fe/Mn-rich $Al_6(Mn,Fe)$ and $Al_m(Mn,Fe)$, in addition to primary Mg_2Si (Fig. 1b). Meanwhile, a minor fraction of Cr-rich α-$Al_{15}(Fe,Mn,Cr)_3Si_2$, ε-$Al_{18}(Cr,Mn)_2Mg_3$, and $Al_6(Mn,Cr)$ phases as well as $Al_7(Cr,Ti)$ (not shown in Fig. 1b) were observed [23]. Low melting-point eutectic phases of τ-Al_6CuMg_4 and β-Al_5Mg_2 were also detected in the interdendritic regions, which were formed during the last stage of solidification.

SEM backscattered images (Fig. 1c-g) show typical intermetallic phase distributions after single-and multi-step treatments. It can be seen that after heat treatment, especially at higher temperature, such as 525 ^oC in industrial homogenization, the majority of the Fe/Mn-rich intermetallics were changed to α-$Al_{15}(Fe,Mn)_3Si_2$ and $Al_6(Mn,Fe)$ with Chinese script morphologies. During heat treatment, primary Mg_2Si was partially or fully dissolved into matrix. As a result, the Si solute level in aluminum matrix becomes higher, which can stabilize the transformation of Fe-rich intermetallics to α-$Al_{15}(Fe,Mn)_3Si$ [24–27]. Moreover, low melting-point eutectic phases such as τ-Al_6CuMg_4 and β-Al_5Mg_2 were

mostly dissolved in all heat treatments except SS348 and 2S-LT samples, where a small fraction remained (Fig. 1c and e) because of the low heat treatment temperature. It should be mentioned that τ-Al_6CuMg_4 and β-Al_5Mg_2 are stable at relatively low temperatures [14]. However, the large diffusion coefficients of Cu and Mg enhance the dissolution rate of these phases at relatively high temperatures [27, 28]. Therefore, they were mostly dissolved after heat treatment. Furthermore, the minor Cr-rich ε-$Al_{18}(Cr,Mn)_2Mg_3$ and $Al_6(Mn,Cr)$ phases were stable after all heat treatments (Fig. 1c to 1g), which can be attributed to their higher formation temperature and the slow diffusion rate of Cr at high temperatures ($D_{400\,°C} = 1.29\times10^{-21}$ [19, 27, 28]). Table 3 displays the quantitative results for the area fractions of the major and minor intermetallic phases in the as-cast and heat-treated conditions, showing a general trend of partial dissolution of all intermetallic phases after various heat treatments. It is evident that the amount of intermetallics decreases with increasing heat treatment temperature. Compared to all heat treatments, I-Homo showed the lowest area fraction of the Fe/Mn-rich phase as well as Mg_2Si (Fig. 1g), which is likely due to the higher treatment temperature.

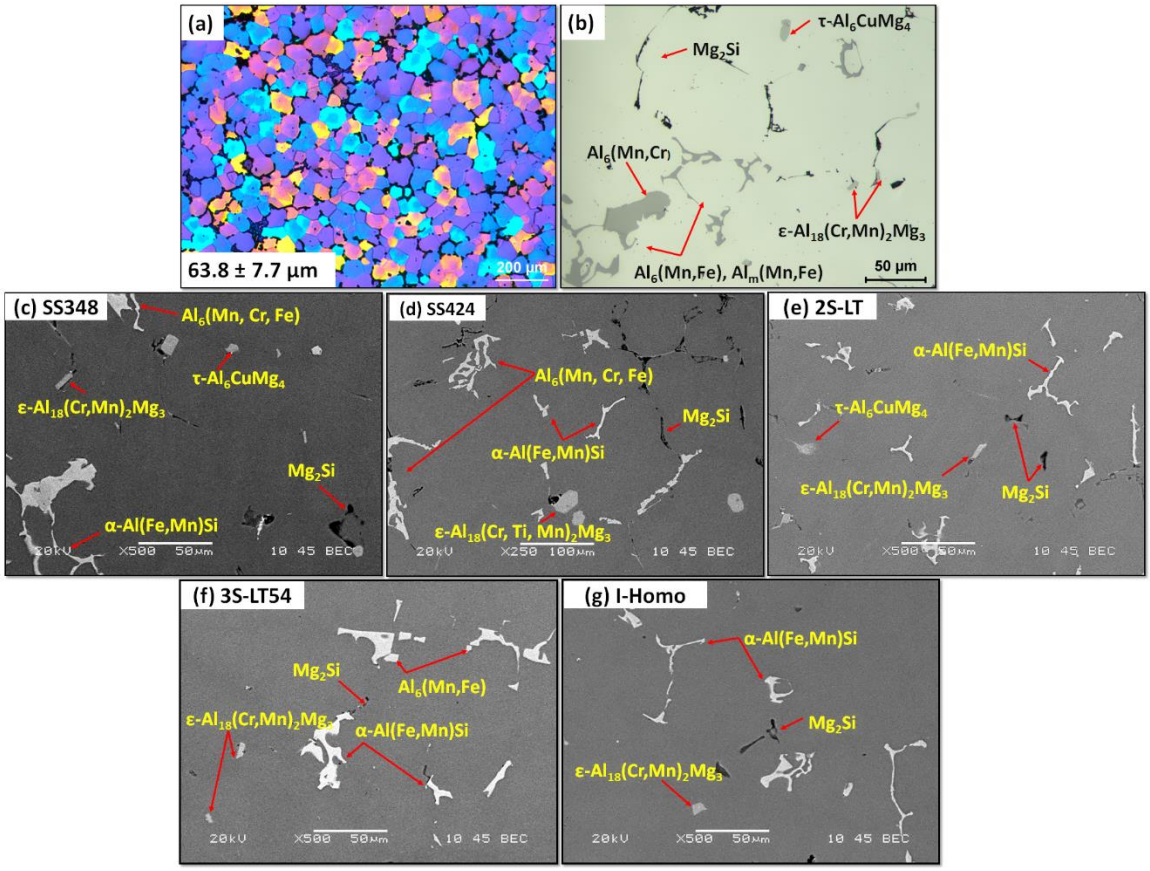

Fig. 1. Optical images for (a): grain structure and (b): distribution of intermetallic phases in as-cast condition while SEM backscattered images for the distribution of intermetallics after various heat treatments: (c) SS348, 375 °C /48 h, (d) SS424, 425 °C /12 h, (e) 2S-LT, 275 °C /12 h + 375 °C /48 h, (f) 3S-LT52, 275 °C /12 h + 375 °C /48 h + 500 °C /4 h and (g) industrial homogenization (I-Homo), 430 °C /2 h + 480 °C /2 h + 525 °C /2 h.

Table 3 Area fraction of intermetallic phases (%) in as-cast and heat-treated conditions

Conditions	Fe/Mn-rich phases	Mg_2Si	Others	Total
As-cast	2.78±1.6	0.82±0.3	0.12±0.1	3.72
SS348	2.45±1.2	0.76±0.4	0.09±0.1	3.3
SS424	2.46±2	0.69±0.5	0.05±0.1	3.2
SS524	2.07±1.6	0.6±0.3	0.04±0.1	2.71
2S-LT	2.18±0.4	0.62±0.1	0.05±0.04	2.85
3S-LT54	1.85±0.7	0.6±0.2	0.05±0.04	2.45
I-Homo	1.46±0.6	0.56±0.2	0.001±0.004	2.021

Note: the last one or two numbers of SS3xx, SS4xx and SS5xx represent the soaking time in h.

3.2 Evolution of dispersoids

3.2.1 Industrial homogenization treatment

Fig. 2 shows the dispersoid distribution after the industrial homogenization treatment (I-Homo sample). As shown in the optical image (Fig. 2a), a number of dispersoids formed in the dendrite cells during homogenization, appearing as the dark DZ regions. In addition, large DFZ areas, appearing as light regions, can be observed surrounding the intermetallic phases. DFZ formation is reported to be due to the depletion of Mn content near the Fe/Mn-rich intermetallics [7]. The area fractions of DFZs and DZs were measured to be 35.9% and 60.7%, respectively. It is assumed that the volume fractions are roughly equivalent to the measured area fractions.

As observed by SEM (Fig. 2b), the dispersoid number density was small while their average size was large in the DZ. In addition to the normal precipitation of dispersoids, another type of rod-like dispersoid precipitated mostly at the edge of the DZ (Fig. 2c). Detailed information about the dispersoids is revealed in the TEM image (Fig. 2d). Two different types of dispersoids with cube- and rod-like morphologies co-existed in the DZ (indicated by red crosses). The selected area diffraction patterns (SADP) of cube- and rod-like dispersoids are shown in Fig. 2e and 2f respectively, while their TEM-EDS results from more than 50 particles are listed in Table 4. It can be found that the cube-like dispersoids have a higher Mn content than that of rod-like ones. Combined the results of SADP and their TEM-EDS as well as information from the literature [5, 13, 17, 29, 30], the cube-like dispersoids seem mostly to be Al_4Mn (Hexagonal, $a=b$=2.812 nm, c =1.274 nm, $\gamma=120^o$ [31]), while the rod-like ones are believed to be Al_6Mn (Orthorhombic, a=0.6498 nm b=0.7574 nm, c =0.887 nm [5, 32]). However, α-Al(Mn,Fe)Si dispersoids were hardly detected in the experimental alloy, which is likely contributed to the higher Mg and Mn contents in the present work [5, 14, 17]. Fe and Cr can easily replace Mn in the dispersoids because of (1) the similar bcc crystal structures of Fe, Cr, and Mn, and (2) their comparable atomic radii. The presence of Cr may improve the thermal stability of dispersoids owing to the slow diffusivity of Cr in Al at relatively high temperatures [27,

28]. Quantitative image analysis showed that the number density of the dispersoids was approximately 66.8 μm^{-3} and the equivalent diameter was ~63 nm, as shown in Table 4.

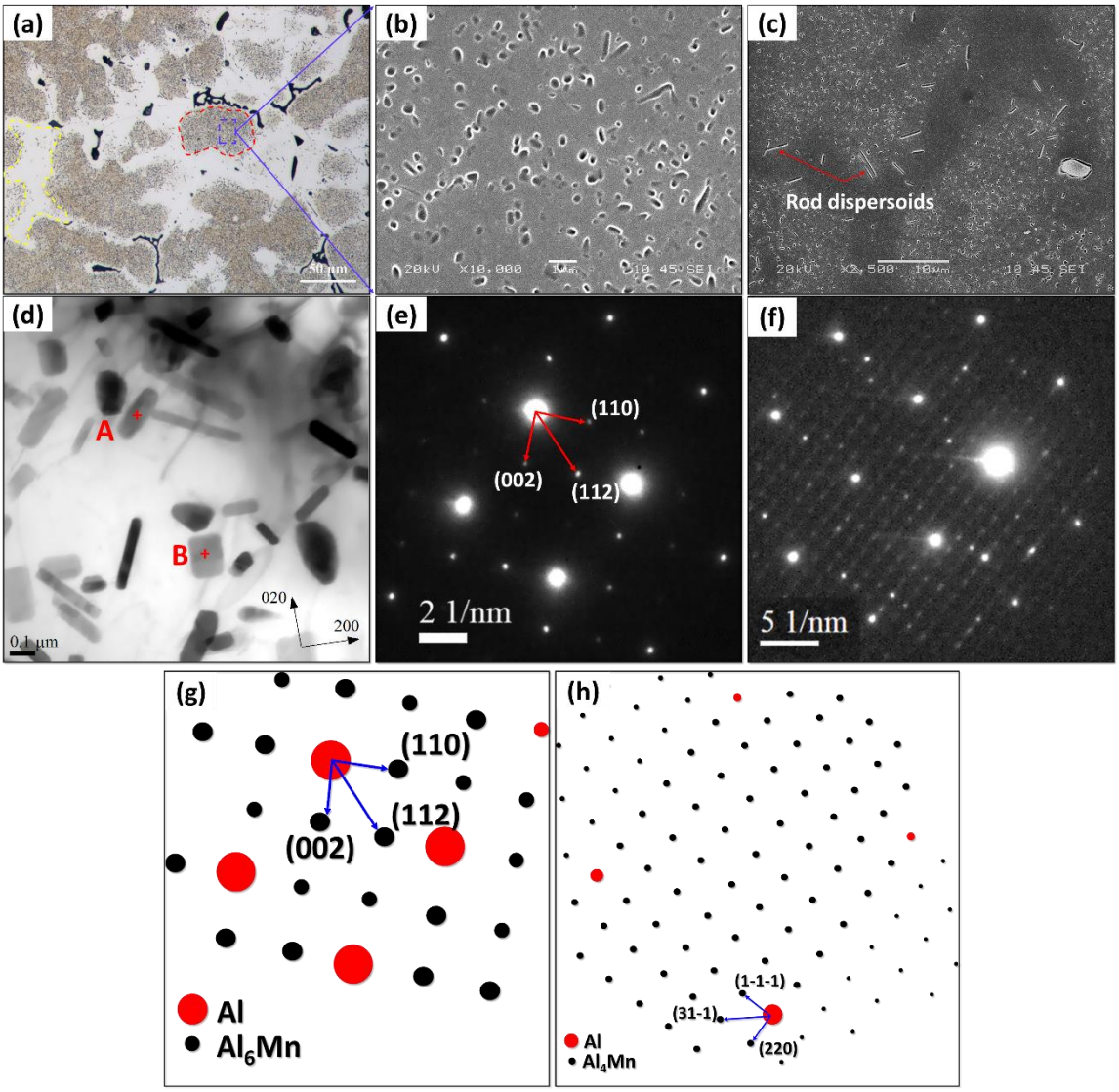

Fig. 2. Microscopy results after industrial homogenization treatment (I-Homo): (a) OM image of DZ and DFZ distributions, (b) dispersoids in DZs under SEM, (c) rod-like dispersoids under SEM, (d) type and morphology of dispersoids revealed by TEM, and (e) TEM-SADP for rod-like particle "A" as Al_6Mn and (f) TEM-SADP for cube-like particle "B" as Al_4Mn as well as the simulated SADP in (g) for Al_6Mn and (h) for Al_4Mn. All the TEM images and SADP are obtained in <001> zone axis of Al.

Table 4 Statistical TEM-EDS results (at.%) of Al_6Mn and Al_4Mn

	Mg	Mn	Cr	Fe	Al
Al_6Mn	5.58±0.5	1.85±0.8	0.36±0.2	0.07±0.2	92.14±0.8
Al_4Mn	3.69±0.9	7.42±1.8	1.04±0.5	0.24±0.3	87.61±1.9

As illustrated in Fig. 2, the dispersoids has a relatively low number density in addition to a large DFZ area fraction after industrial homogenization at high temperature. A large volume fraction of finer dispersoids is vital for improving the mechanical properties of 5xxx alloys. Consequently, various single- and multistep heat treatments were applied to study the precipitation behavior of dispersoids.

3.2.2 Single-step heat treatment

To determine the formation behavior of dispersoids in the experimental alloy, single-step heat treatments (SS3xx, SS4xx, and SS5xx in Table 2) with different soaking times were initially performed. In general, electrical conductivity (EC) and microhardness measurements are two essential methods for evaluating the precipitation behavior of dispersoids [7, 31]. Fig. 3 shows the values of EC and microhardness after various single-step heat treatments. As shown in Fig. 3a, the lowest EC (19.1% IACS) was obtained in the as-cast condition, indicating that a high level of supersaturation in the aluminum matrix was reached. For the heat-treated samples, EC rapidly increases with increasing treatment temperature and time, signifying the decomposition of the α-Al supersaturated solid solution and the formation of dispersoids.

When heat-treated at 375 °C (Fig. 3a), the EC continued to increase even after 48h, indicating the continuous decomposition of the solid solution and precipitation of dispersoids. With increasing treatment temperature (425 and 500 °C), the EC reached its peak value within a short time (24 h at 425 °C and 12 h at 500 °C), indicating the complete precipitation of dispersoids. In addition, the EC slightly decreased after 12 h at 500 °C, which is mainly attributed to the dissolution of low eutectic melting phases (τ-Al_6CuMg_4/β-Al_5Mg_2) and primary Mg_2Si phase at high treatment temperatures, as shown in Table 3.

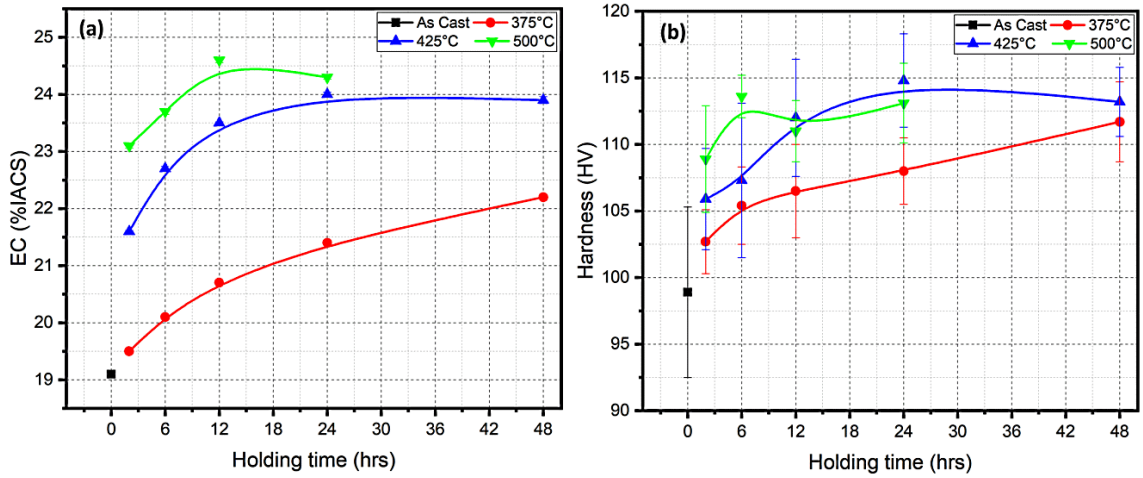

Fig. 3. (a) Electrical conductivity and (b) microhardness after single step heat treatments.

Fig. 3b shows the microhardness after single-step heat treatments. As observed, the microhardness after all heat treatments was generally higher than that of the as-cast condition. Furthermore, a similar tendency with EC also exists. When treated at 375 °C, the microhardness shows a continuous increase with increasing holding time, indicating a strengthening effect by the precipitation of dispersoids. At high treatment temperatures (425 and 500 °C), the microhardness values first increased with the holding time and reached a maximum value after 24 h at 425 °C and 6 h at 500 °C, followed by a slight decrease with a further increase in the soaking time. This implies that the maximum strengthening effect of the dispersoid precipitation is reached at a certain soaking time at both temperatures. When further treated at 500 °C for a prolonged time (24 h), a slight increase in the microhardness was observed, which is likely due to the increase in solid solution strengthening by the dissolution of low melting-point eutectic phases, as confirmed by the 500 °C EC values.

The evolution of EC and microhardness in Fig. 3 is likely ascribed to the precipitation behavior of the dispersoids during various heat treatments. Fig. 4 displays typical microstructures showing the distribution of dispersoids after the three single-step heat treatments. Table 5 summarizes the quantitative image analysis of DZs, DFZs, and dispersoids. When treated at 375 °C for 6 h (Fig. 4a), the precipitation of dispersoids was not obvious, and the dispersoids appeared sparsely within the matrix. After 48 h at 375 °C, the DZ and DFZ became more visible (Fig. 4b), and continuous precipitation of fine dispersoids from the matrix was observed (Fig. 4c). As shown in Table 4, the volume fraction of DZ significantly increased from 33.3 vol.% after 375 °C/6 h to 64.4 vol.% after 375 °C/48 h with a remarkable decrease in the volume fraction of DFZ. The number density of the dispersoids after 375 °C/6 h is only 87 μm^{-3}, which increased significantly to 325 μm^{-3} after 375 °C/48 h.

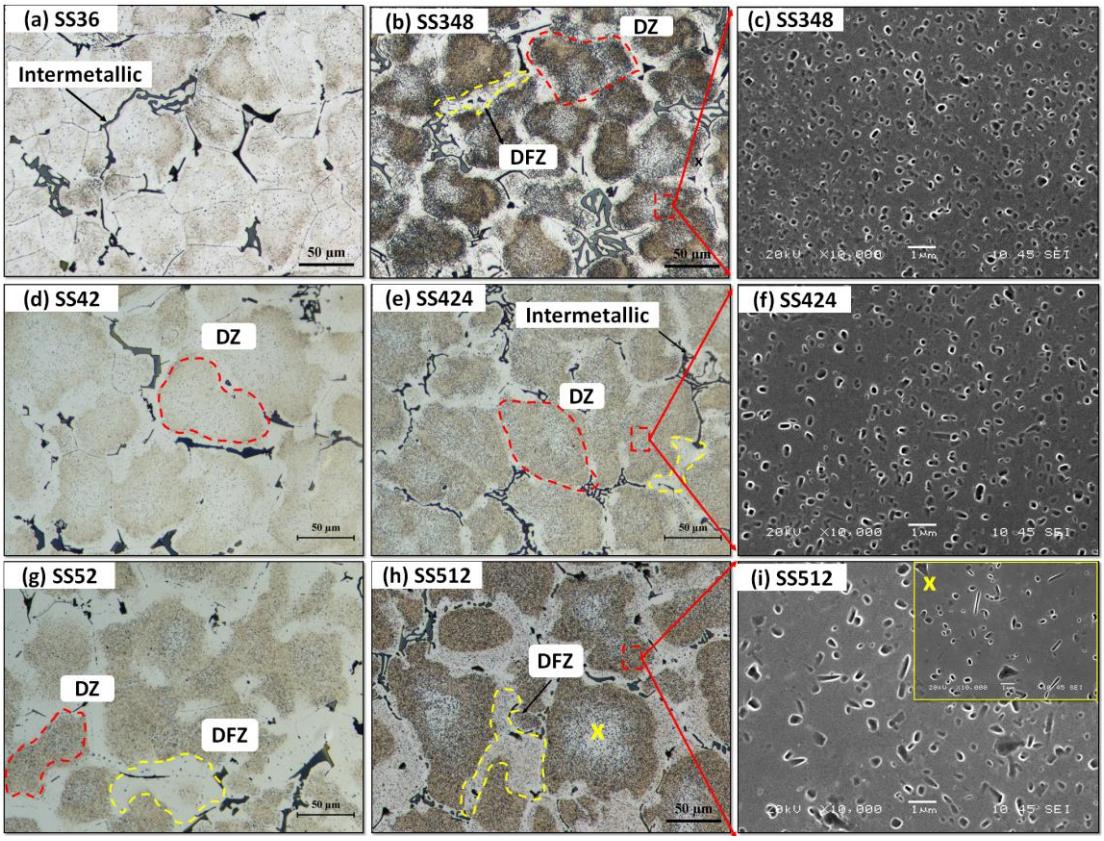

Fig. 4. Typical microstructures showing the dispersoid distribution after single step heat treatments: (a-c) SS3xx treatment at 375 °C: (a) optical image for 6 h, (b)optical image for 48 h and (c) SEM image for 48 h ; (d-f) SS4xx treatment at 425 °C: (d) optical image for 2 h, (e) optical image for 24 h and (f) SEM image for 24 h; (g-i) SS5xx treatment at 500 °C (g–i): (g) optical image for 2 h, (h) optical image for 12 h and (i) SEM image for 12 h

Table 5 : Characteristics of DZ, DFZ and dispersoids during precipitation heat treatments

Conditions	Volume fraction %		Equivalent diameter, nm	Number density, μm^{-3}
	DZ	DFZ		
SS36	33.3 ± 1.7	62.5 ± 1.5	14.4 ± 2.3	87 ± 24.3
SS348	64.4 ± 2.7	30.2 ± 1.6	24.4 ± 2	325 ± 47
SS424	68.8 ± 1	26.2 ± 1	35.6 ± 3	188.1± 24
SS56	65.1 ± 1.1	30.8 ± 1.7	47.2 ± 5	137 ± 35.5
SS512	62.4 ± 1.2	35.1 ± 1.3	51.4 ± 9	90.4 ± 27.9
I-Homo	60.7±2.1	35.9±3.4	63±12.5	66.8±12.7

With increasing treatment temperature, the DZ and DFZ were already visible after 2 h at 425 °C (Fig. 4d) and 500 °C (Fig. 4g), indicating the efficient precipitation of dispersoids from the decomposition of the supersaturated solid solution. When treated at 425 °C for 24

h (Fig. 4e), the full precipitation of dispersoids was reached (Fig. 4f). The distribution of dispersoids is more uniform than that of the sample treated at low temperature (375 °C for 48 h), as indicated by the increase in DZ (68.8 vol.% after 425 °C/24 h vs. 64.4 vol.% after 375 °C/48 h) and the corresponding decrease in DFZ. However, the size of the dispersoids increased and the number density decreased relative to that of the sample treated at 375 °C for 48 h (Table 5).

When treated at a high temperature with a longer soaking time (500 °C/12 h), some dispersoid-depleted zones appeared in the center of the dendrite cells, as marked with an X in Fig. 4h, where the number density of the dispersoids was considerably lower than the surrounding areas of the dendrite cells. This suggests that after the full precipitation (6 h, see Fig. 3), dissolution and coarsening of dispersoids occurred with prolonged soaking time at high treatment temperature. This was confirmed by the decrease in the microhardness after treatment at 500 °C/6 h (Fig. 3b). SEM observations (Fig. 4i) show that the dispersoids were much larger in size and lower in number density than those treated at 375 °C/48 h and 425 °C/24 h.

Detailed information on the dispersoids in the DZ after various heat treatments was studied using TEM, and the results are shown in Fig. 5.

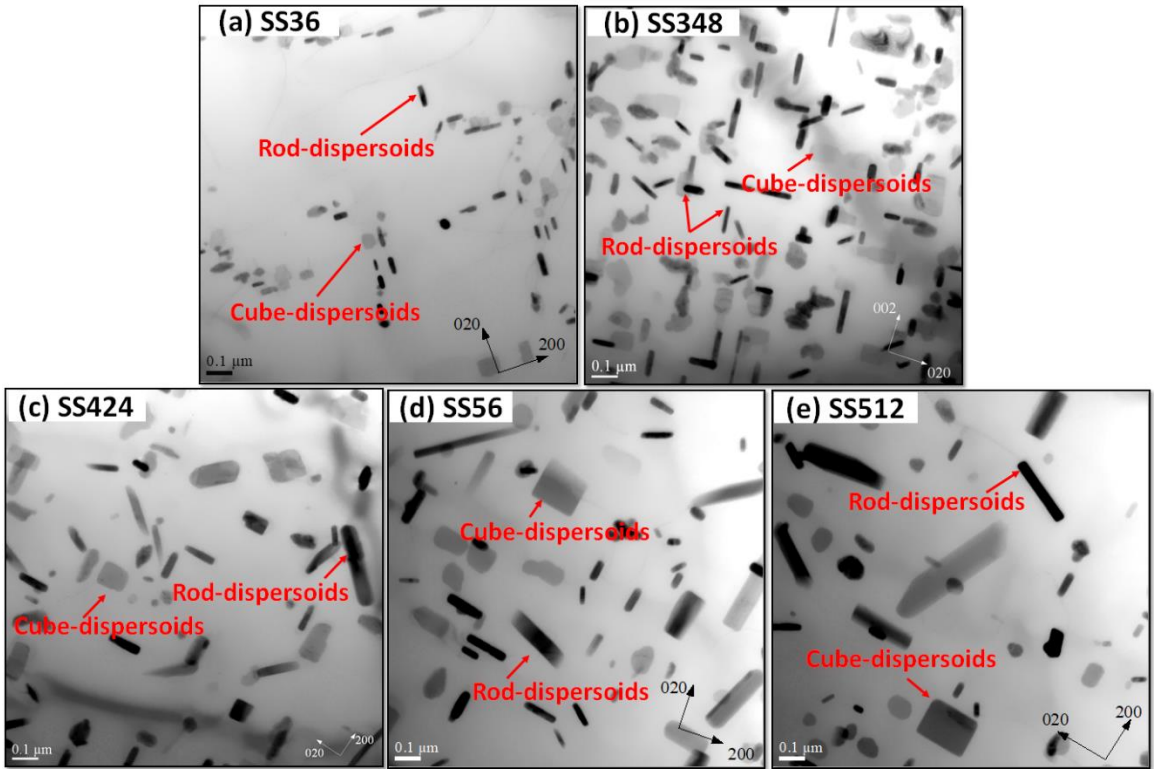

Fig. 5. Bright-field TEM images showing the size, type and morphology of dispersoids after single-step heat treatments: (a) 375 °C/6 h, (b) 375 °C/48 h, (c) 425 °C/24 h, (d) 500 °C/6 h and (e) 500 °C/12 h.

In general, two types of dispersoids with cube- and rod-like morphologies were observed under all heat treatment conditions. As illustrated in Fig. 5a, only a small number of fine dispersoids was observed after 375 °C/6 h, which explains the slight increase in the EC and microhardness (Fig. 3). When the holding time was increased to 48 h (Fig. 5b), a large number density of the dispersoids appeared. The number density increased from 87 μm^{-3} at 375 °C/6 h to 325 μm^{-3} at 375 °C/48 h (Table 5). With increasing treatment temperature (425 and 500 °C), the dispersoids precipitated out with a larger size and lower number density, as depicted in Fig. 5c-d, when compared with the sample at 375 °C/48 h (Fig. 5b). This can be attributed to the fast growth and coarsening of dispersoids owing to the high diffusion rate of Mn and Fe at relatively high temperatures [27, 28]. For instance, the equivalent diameter of dispersoids increases from 24.4 nm after 375 °C/48 h to 35.6 nm after 425 °C/24 h and further to 47.2 nm after 500 °C/6 h. However, the number density of the dispersoids was reduced from 325 μm^{-3} after 375 °C/48 h to 188 μm^{-3} after 425 °C/24 h and further to 137 μm^{-3} after 500 °C/6 h. With heat treatment at a high temperature of 500 °C, the coarsening of the dispersoids was significant (Fig. 5e). The number density further decreased to 90.4 μm^{-3} and the size increased to 51.4 nm after 500 °C/12 h.

3.2.3 Multistep heat treatments

To improve the mechanical properties of 5xxx alloys, it is necessary to reduce the size of the dispersoids as well as increase their volume fraction. Therefore, the concept of multistep heat treatments is introduced to optimize the formation of dispersoids and to adapt to the rolling process.

Previous studies have reported that the pre-existing metastable β'-MgSi that formed during the first step (250 °C/24 h) could act as nucleation sites for Mn-bearing dispersoids, and therefore, the precipitation of dispersoids after the second step (375 °C/48 h) was greatly promoted in 3xxx alloys [10, 11]. In the present study, a similar two-step treatment approach (2S-LT, 275 °C/12 h + 375 °C/48 h) was first explored with the aim of achieving a high nucleation rate of dispersoids at a relatively low temperature (the first step) followed by the decomposition of the supersaturated solid solution and the precipitation of dispersoids in the second step at 375 °C/48 h.

Fig. 6 shows the distribution of the dispersoids during the 2S-LT heat treatment. Fig. 6a shows a bright-field TEM image after the first-step treatment (275 °C/12 h), where a large number of plate-like precipitates appeared with a length range of 280–430 nm and a width of 24–32 nm, which were identified as β'-MgSi [10, 32]. When the samples continued to be treated at 375 °C/48 h, the formation of dispersoids became more obvious with a large fraction of DZ (marked with a red dotted line) in addition to a small fraction of DFZ (marked with a yellow line), as shown in the optical image in Fig. 6b. Most β'-MgSi was dissolved during the second step, and fine dispersoids precipitated along $[001]_{Al}$, which is the preferred orientation of metastable β'-MgSi (Fig. 6c). The dispersoids were finer with an equivalent diameter of 22.4 nm, and their number density was higher (741.8 μm^{-3}), as shown in Table 5, compared with those after the single-step treatment (SS348 in Table 4, 375 °C/48 h). This confirms the promotion effect of the dispersoid precipitation resulting from the pre-formed β' in the first step. As a result, the microhardness after 2S-

LT was remarkably higher (121.5 HV) than that of the single-step treatment (112 HV in SS348).

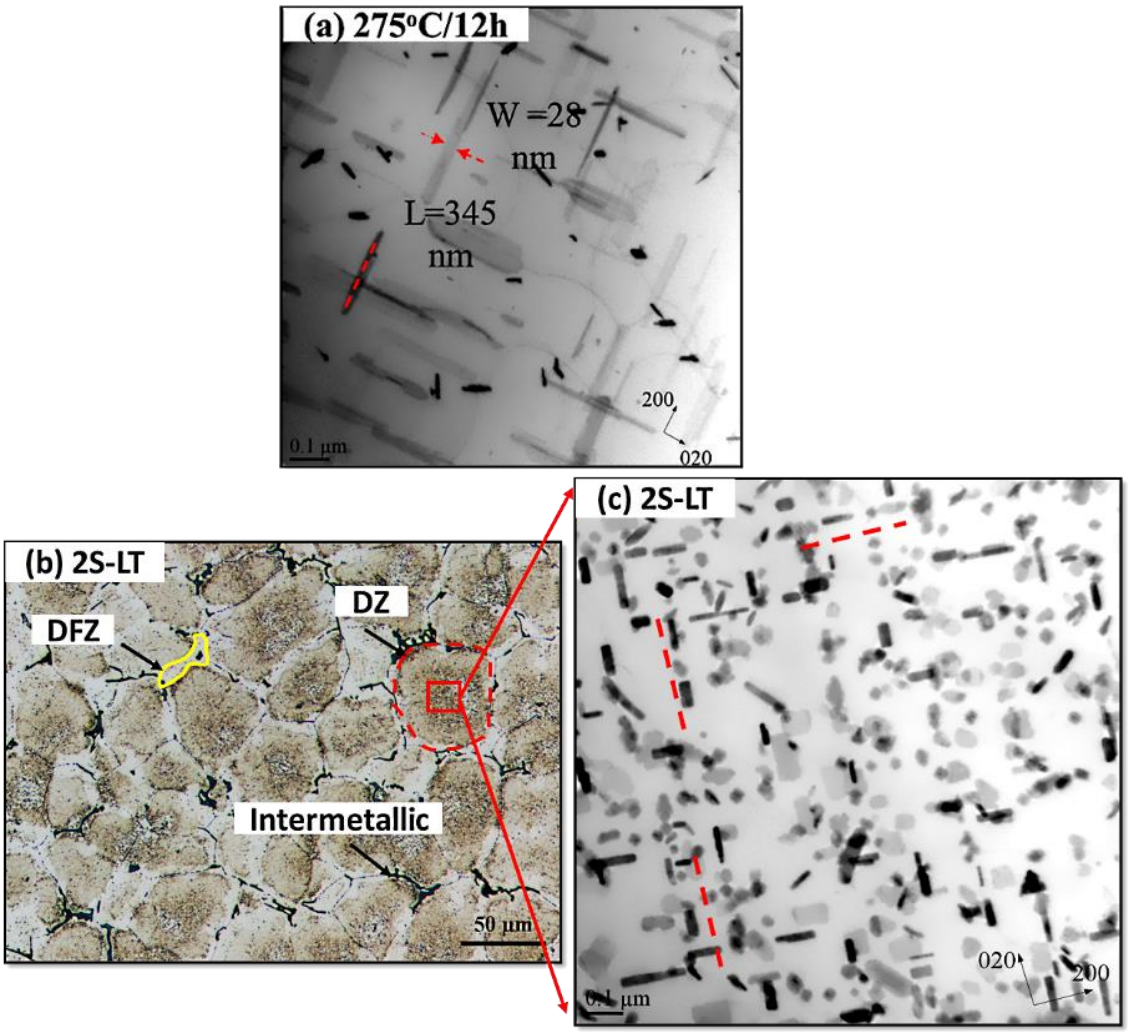

Fig. 6. Distribution of dispersoids during two-step treatment (2S-LT, 275 °C/12 h + 375 °C/48 h): (a) bright-field TEM image showing the precipitation of β'-Mg_2Si after the first step, (b) optical image of the DZ and DFZ distribution, and (c) bright-field TEM image showing the dispersoid precipitation along $[001]_{Al}$ after the second step.

Although the 2S-LT treatment resulted in a higher number density of finer dispersoids, there were still some undissolved low-eutectic melting phases, as shown in Fig. 1d and Table 3, which could cause difficulties during the hot rolling process. Therefore, two other conditions with the last step at relatively high temperature (500 °C) were also studied, namely 2S-HT (425 °C/24 h + 500 °C/4 h) and 3S-LT54 (275 °C/12 h + 375 °C/48 h + 500 °C/4 h).

Fig. 7 shows the distribution of the dispersoids after the 2S-HT and 3S-LT54 heat treatments. An overview of the DZ and DFZ distribution in the 2S-HT and 3S-LT54 samples is shown in Fig. 7a and 7c. With increasing temperature in the last step at 500 °C, an obvious DFZ increase was observed compared to the same conditions without the last step. Furthermore, the TEM images in Fig. 7b and 7d reveal that the dispersoids coarsened in the last step, owing to the high diffusivity of Mn and Fe at high temperatures [27, 28]. For instance, the dispersoids were much coarser with a lower number density when treated at 2S-HT (Fig. 7b) relative to the SS424 sample (Fig. 5c). Similarly, the 3S-LT54 sample exhibited a remarkable increase in dispersoid size with a lower number density (Fig. 7d) compared with the 2S-LT sample (Fig. 6c). Table 6 summarizes the quantitative analysis of the dispersoids after the three multi-step heat treatments. It can be seen that the DFZ volume fraction increases from 26 vol.% after SS424 to 30.4 vol.% after 2S-HT, while the DFZ volume fraction increases from 26.1 vol.% after 2S-LT to 28.9 vol.% after 3S-LT54. On the other hand, the dispersoid size increases from 22.4 nm after 2S-LT to 31 nm after 3S-LT54, along with a remarkable reduction in their number density. However, the dispersoids were much finer and their number density was considerably higher after treatment at 3S-LT54 than after 2S-HT.

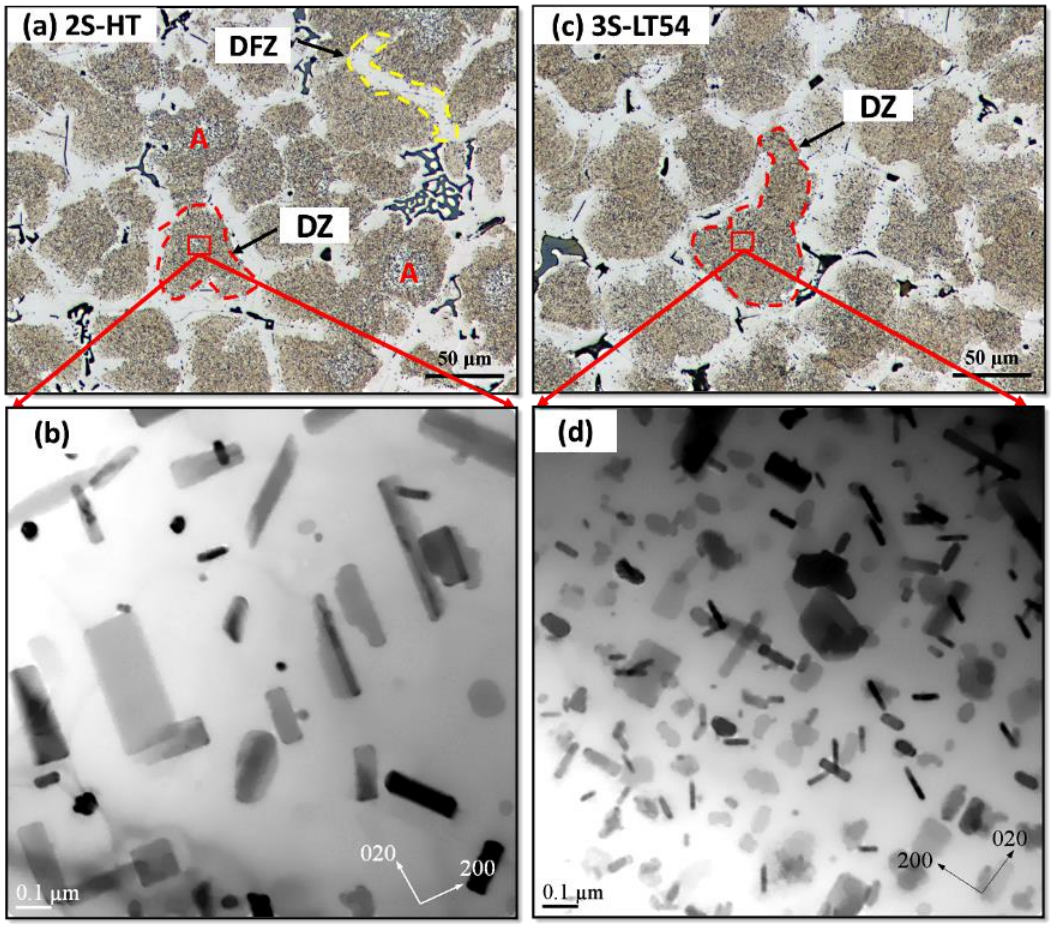

Fig. 7. Distribution of dispersoids (a and b) after the two-step heat treatment (2S-HT) and (c and d) the three-step heat treatment (3S-LT54); a and c are OM images, and b and d are TEM images.

Table 6. Characteristics of DZ, DFZ and dispersoids after multi-step heat treatments

Conditions	Volume fraction %		Equivalent diameter, nm	Number density, μm^{-3}
	DZ	DFZ		
2S-LT	70.9±2	26.1±2	22.4 ± 8	741.8 ± 65.2
2S-HT	67.1±1.5	30.4±2.4	55.2 ± 7	155.4 ± 11.5
3S-LT54	67.7±1.1	28.9±1.1	31.1 ± 4	333.3 ± 75

Fig. 8 summarizes the microhardness measurement results. It can be seen that the microhardness significantly increases after all heat treatments compared with the as-cast condition, reflecting the strengthening effect of the dispersoid precipitation. However, the benefit of the two-step treatments is dependent on the condition applied. For instance, the microhardness after the two-step treatment (2S-LT) is remarkably higher than that of the single-step treatment (SS348), while there is no significant difference in microhardness between the 2S-HT and SS424 samples. As shown in Fig. 8, the microhardness shows a slight decrease after 3S-LT54 compared with 2S-LT (118 vs. 121 HV), which can be explained by a decreasing dispersoid number at the last step (Fig. 7d vs. Fig. 6c). However, the microhardness of the 3S-LT54 sample is still higher than those treated with 2S-HT and I-Homo conditions, indicating the strong strengthening effect of fine and densely-distributed dispersoids (Tables 5 and 6).

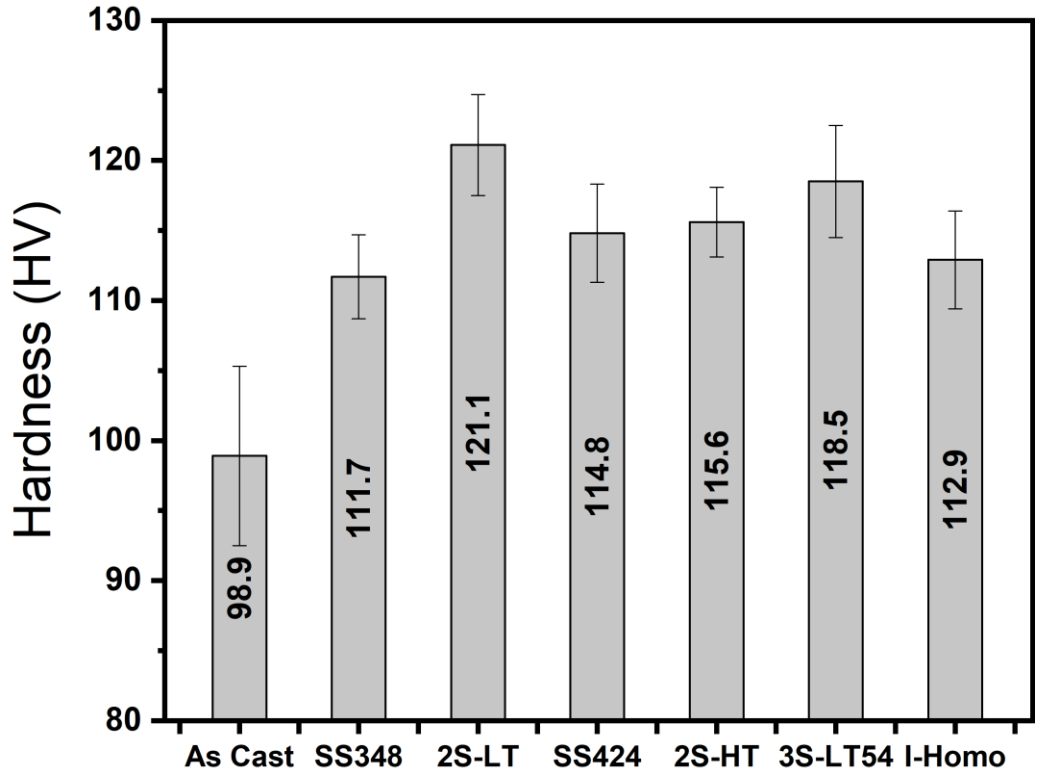

Fig. 8. Microhardness measurements after single and multi-step heat treatments.

3.3 Rolling Performance

Al-Mg-Mn 5xxx alloys are usually used in sheet form fabricated by the hot rolling process. Hot rolling trials of heat-treated cast ingots were performed; these samples included those that had undergone SS348, SS424, and multi-step treatments. Fig. 9 shows representative views of the rolled samples. As shown in Fig. 9a, the hot-rolled samples of SS348, SS424, and 2S-LT exhibited severe problems with alligator and surface cracks after only 4–6 passes with an area reduction of 24%–36%. This can most likely be attributed to the remaining low-melting eutectic intermetallic phases resulting from the relatively low heat treatment temperatures (375–425 °C) [33, 34]. However, as shown in Fig. 9b, the samples exposed to 2S-HT, 3S-LT54, and I-Homo treatments exhibited good rolling performance with acceptable surface conditions down to the final sheet thickness of 3.2 mm (88% reduction). All three heat treatments involved a final step at a high temperature of 500 °C, which effectively dissolved the low-melting eutectic intermetallic phases and hence reduced the sensitivity to alligator problems and surface cracks. In addition, coarse rod-like dispersoids were observed in the peripheral areas of the DFZs after high-temperature heat treatments, such as 2S-HT, 3S-LT54, and I-Homo treatments, as shown in Fig. 2c and Fig. 10. A previous study has reported that the precipitation of rod-like dispersoids in DFZs could provide a uniform slip distribution during hot deformation, and hence reduce the local stresses at the grain boundaries, resulting in a high resistance to intergranular fracture and alligator problems [33].

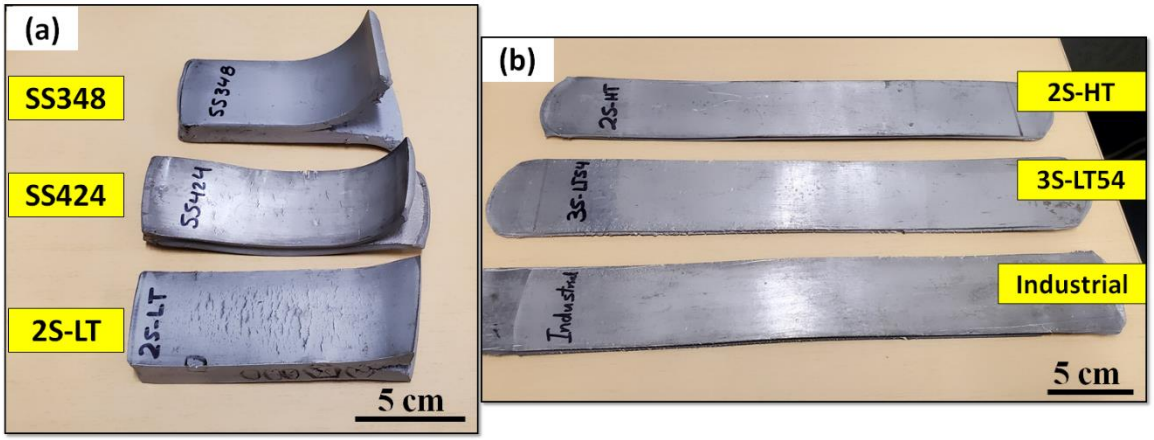

Fig. 9. Representative views of rolled samples with various heat treatments: (a) samples with alligator and surface crack problems and (b) samples with good rolling performance.

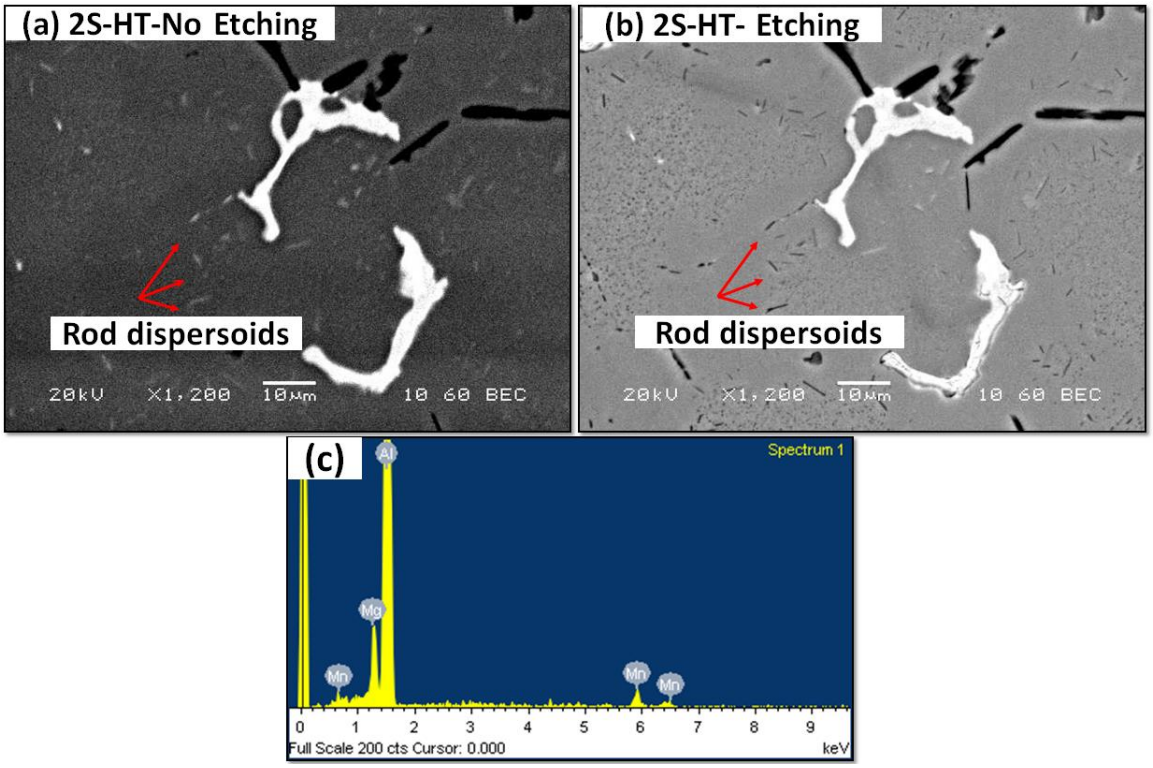

Fig. 10. Precipitation of rod-like dispersoids in DFZs after high temperature treatment of the 2S-HT sample: SEM images (a) before and (b) after etching, and (c) SEM-EDS result.

3.4 Tensile properties after hot rolling

Prior to tensile testing, the hot-rolled samples were annealed at 300 °C/5 h to release the thermal stresses induced by rolling. Fig. 11 shows the room-temperature tensile properties of the rolled samples with good rolling performance. As observed, both the 2S-HT and 3S-LT54 samples have higher tensile strengths (YS and UTS) than the I-Homo samples. The YS and UTS of the 3S-LT54 rolled samples reached 178 and 331 MPa, respectively, showing an improvement of 7.9% in YS and 6.3% in UTS relative to the I-Homo samples at the same elongation level.

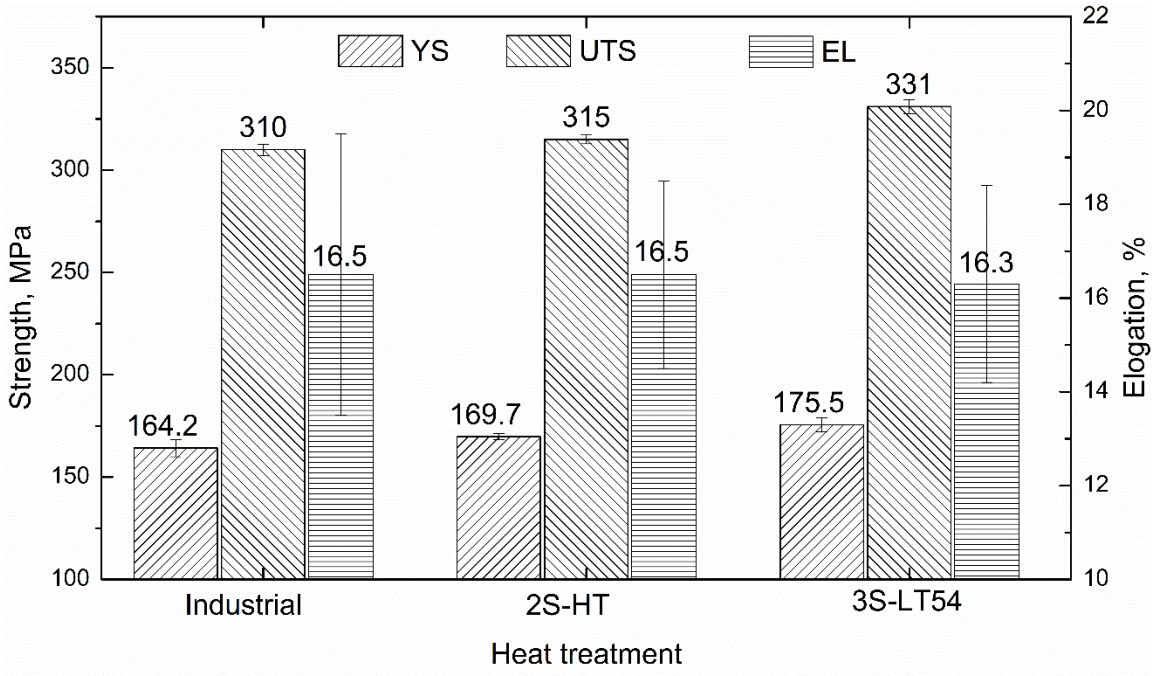

Fig. 11: Tensile properties of three rolled sheet samples.

Fig. 12 shows the microstructure after annealing of the hot-rolled samples subjected to 3S-LT54 and I-Homo treatments. Both samples exhibit elongated grains parallel to the rolling direction. However, the I-Homo sample (Fig. 12b) shows a higher DFZ area fraction than the sample after 3S-LT54 (Fig. 12b). At the higher magnification of the SEM images (Figs. 12c and d), it can be seen that the dispersoids in the 3S-LT54 sample have a higher number density with a finer size (Fig. 12c) compared to the I-Homo sample. The fact that the rolled 3S-LT54 samples possess higher tensile strengths relative to the I-Homo samples indicates a reasonable strengthening contribution from the fine dispersoids, providing an alternative way to improve the mechanical properties of non-heat-treatable 5xxx wrought alloys. The challenge of maximizing this additional dispersoid strengthening can be addressed through appropriate alloy chemistry, heat treatment, and rolling processes targeted toward maintaining fine and densely distributed dispersoids in the microstructure.

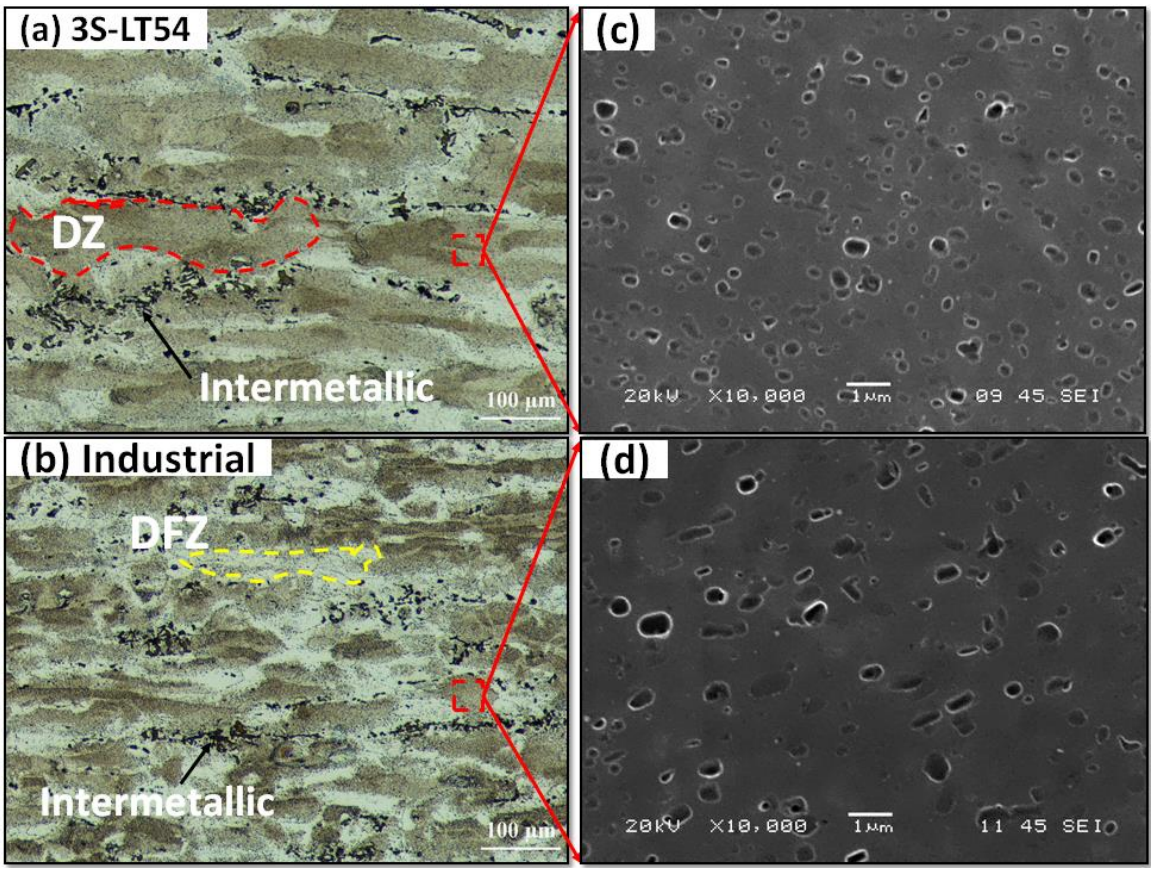

Fig. 12. Microstructures after hot-rolling of the samples: a and c for 3S-LT54 while (b and d for I-Homo treatments;(a and b are OM images, and c and d are SEM images).

4. Conclusions

In the present study, various single- and multistep heat treatments were performed to optimize the characteristics of the dispersoids in terms of the size, number density, and distribution in an Al-5% Mg-0.8% Mn alloy. The rolling performance after different heat treatments was also evaluated. The following conclusions can be drawn:

- The as-cast microstructure of Al-5% Mg-0.8% Mn alloy consisted of aluminum dendrite cells surrounded by dominant Fe/Mn-rich Al_6(Mn,Fe) and Al_m(Mn,Fe) intermetallic phases, in addition to primary Mg_2Si. Minor fractions of Cr-rich α-Al_{15}(Fe,Mn,Cr)$_3Si_2$, ε-Al_{18}(Cr,Mn)$_2Mg_3$, and Al_6(Mn,Cr), as well as a low melting-point eutectic τ-Al_6CuMg_4 phase were also detected in the interdendritic regions.
- During all heat treatments, a number of cube- and rod-like dispersoids were observed to precipitate in the dendritic cells and grains. Two types of Mn-bearing dispersoids, Al_4Mn and Al_6Mn, were identified based on their morphology and chemical composition. The size, number density, and distribution of the dispersoids were strongly dependent on the heat treatment step, temperature, and time.
- The low-temperature two-step heat treatment (2S-LT, 275 °C/12 h + 375 °C/48 h) generated the highest number density of dispersoids with the finest size among all heat treatments studied, but severe defects were created during the hot rolling process.

- The three-step heat treatment (3S-LT54, 275 °C/12 h + 375 °C/48 h + 500 °C/4 h) provided the best combination of dispersoid characteristics and rolling performance.
- The mechanical properties of rolled sheets subjected to the three-step heat treatment (3S-LT54) were improved over those obtained through the industrial homogenization treatment, owing to the higher number density and finer size of dispersoids, providing an alternative way to improve the mechanical properties of non-heat-treatable 5xxx wrought alloys.

Acknowledgments

The authors would like to acknowledge the financial support of the Natural Sciences and Engineering Research Council of Canada (NSERC) under the Grant No. CRDPJ 514651-17 and Rio Tinto Aluminum through the Research Chair in the Metallurgy of Aluminum Transformation at University of Quebec at Chicoutimi.

Data availability: The raw/processed data required to reproduce these findings cannot be shared at this time as the data also forms part of an ongoing study.

References

[1] J.R. Davis, "Aluminum and Aluminum Alloys", *Light Met. Alloy.*, p. 66, 2001, https://doi.org/10.1361/autb2001p351.

[2] J.A. Van Der Hoeven, L. Zhuang, B. Schepers, P. De Smet, J.P. Baekelandt, "A new 5xxx series alloy developed for automotive applications", *SAE Tech. Pap.*, no. 724, pp. 1–8, 2002, https://doi.org/10.4271/2002-01-2128.

[3] Ø. Ryen, B. Holmedal, O. Nijs, E. Nes, E. Sjölander, H.-E. Ekström, "Strengthening mechanisms in solid solution aluminum alloys", *Metall. Mater. Trans. A*, vol. 37, no. 6, pp. 1999–2006, 2006, https://doi.org/10.1007/s11661-006-0142-7.

[4] E.L. Huskins, B. Cao, K.T. Ramesh, "Strengthening mechanisms in an Al-Mg alloy", *Mater. Sci. Eng. A*, vol. 527, no. 6, pp. 1292–1298, 2010, https://doi.org/10.1016/j.msea.2009.11.056.

[5] Y.J. Li, W.Z. Zhang, K. Marthinsen, "Precipitation crystallography of plate-shaped Al6(Mn, Fe) dispersoids in AA5182 alloy", *Acta Mater.* vol. 60, pp. 5963–5974, 2012, https://doi.org/10.1016/j.actamat.2012.06.022.

[6] A.M.F. Muggerud, E.A. Mørtsell, Y. Li, R. Holmestad, "Dispersoid strengthening in AA3xxx alloys with varying Mn and Si content during annealing at low temperatures", *Mater. Sci. Eng. A*, vol. 567, pp. 21–28, 2013, https://doi.org/10.1016/j.msea.2013.01.004.

[7] K. Liu, X.G. Chen, "Development of Al-Mn-Mg 3004 alloy for applications at elevated temperature via dispersoid strengthening", *Mater. Des.*, vol. 84, pp. 340–350, 2015, https://doi.org/10.1016/j.matdes.2015.06.140.

[8] Z. Li, Z. Zhang, X.G. Chen, "Microstructure, elevated-temperature mechanical properties and creep resistance of dispersoid-strengthened Al-Mn-Mg 3xxx alloys with varying Mg and Si contents", *Mater. Sci. Eng. A*, vol. 708, no. October, pp. 383–394, 2017, https://doi.org/10.1016/j.msea.2017.10.013.

[9] Y.J. Li, A.M.F. Muggerud, A. Olsen, T. Furu, "Precipitation of partially coherent α-Al(Mn,Fe)Si dispersoids and their strengthening effect in AA 3003 alloy", *Acta Mater.*, vol. 60, no. 3, pp. 1004–1014, https://doi.org/10.1016/j.actamat.2011.11.003.

[10] K. Liu, H. Ma, X.G. Chen, "Improving the Elevated-Temperature Properties by Two-Step Heat Treatments in Al-Mn-Mg 3004 Alloys", *Metall. Mater. Trans. B Process Metall. Mater. Process. Sci.*, vol. 49, no. 4, pp. 1588–1596, 2018, https://doi.org/10.1007/s11663-018-1268-x.

[11] Z. Li, Z. Zhang, X.G. Chen, "Effect of Metastable Mg_2Si and Dislocations on α-Al(MnFe)Si Dispersoid Formation in Al-Mn-Mg 3xxx Alloys", *Metall. Mater. Trans. A Phys. Metall. Mater. Sci.*, vol. 49, no. 11, pp. 5799–5814, 2018, https://doi.org/10.1007/s11661-018-4852-4.

[12] J. Rakhmonov, K. Liu, P. Rometsch, N. Parson, X.G. Chen, "Effects of Al(MnFe)Si dispersoids with different sizes and number densities on microstructure and ambient/elevated-temperature mechanical properties of extruded Al–Mg–Si AA6082 alloys with varying Mn content", *J. Alloys Compd.*, vol. 861, p. 157937, 2021, https://doi.org/10.1016/j.jallcom.2020.157937.

[13] K. Kannan, J.S. Vetrano, C.H. Hamilton, "Effects of alloy modification and thermomechanical processing on recrystallization of Al-Mg-Mn alloys", *Metall. Mater. Trans. A Phys. Metall. Mater. Sci.*, vol. 27, no. 10, pp. 2947–2957, 1996, https://doi.org/10.1007/BF02663844.

[14] O. Engler, S. Miller-Jupp, "Control of second-phase particles in the Al-Mg-Mn alloy AA 5083", *J. Alloys Compd.*, vol. 689, pp. 998–1010, 2016, https://doi.org/10.1016/j.jallcom.2016.08.070.

[15] P. Ratchev, B. Verlinden, P.V.A.N. Houtte, "Effect of preheat temperature on the orientation relationship of (Mn, Fe)Al6 precipitates in an AA5182 Aluminum-Magnesium alloy", *Acta Metall. mater.*, vol. 43, no. 2, pp. 621–629, 1995.

[16] O. Engler, Z. Liu, K. Kuhnke, "Impact of homogenization on particles in the Al-Mg-Mn alloy AA 5454-Experiment and simulation", *J. Alloys Compd.*, vol. 560, pp. 111–122, 2013, https://doi.org/10.1016/j.jallcom.2013.01.163.

[17] O. Engler, K. Kuhnke, J. Hasenclever, "Development of intermetallic particles during solidification and homogenization of two AA 5xxx series Al-Mg alloys with different Mg contents", *J. Alloys Compd.*, vol. 728, pp. 669–681, 2017, https://doi.org/10.1016/j.jallcom.2017.09.060.

[18] T. Radetić, M. Popović, E. Romhanji, "Microstructure evolution of a modified AA5083 aluminum alloy during a multistage homogenization treatment", *Mater. Charact.*, vol. 65, pp. 16–27, 2012, https://doi.org/10.1016/j.matchar.2011.12.006.

[19] O. Engler, K. Kuhnke, K. Westphal, J. Hasenclever, "Impact of chromium on the microchemistry evolution during solidification and homogenization of the Al-Mg alloy AA 5052", *J. Alloys Compd.*, vol. 744, pp. 561–573, 2018, https://doi.org/10.1016/j.jallcom.2018.02.125.

[20] C. Li, K. Liu, X.G. Chen, "Improvement of elevated-temperature strength and recrystallization resistance via Mn-containing dispersoid strengthening in Al-Mg-Si 6082 alloys", *J. Mater. Sci. Technol.*, vol. 39, pp. 135–143, 2020, https://doi.org/10.1016/j.jmst.2019.08.027.

[21] K.M. Gatenby, J. Creek, D. Kang, S.K. Das, (12) Patent Application Publication

(10) Pub . No .: US 2016 / 0355915 A1, 1 2016.
[22] S.M.Allen, "Foil thickness measurements from convergent-beam diffraction patterns", *Philos. M.*, vol. 43, no. (2), p.325–335, 1981.
[23] A.Y. Algendy, K. Liu, X.-G. Chen, "Formation of intermetallic phases during solidification in Al-Mg-Mn 5xxx alloys with various Mg levels", *MATEC Web Conf.*, vol. 326, p. 02002, 2020, https://doi.org/10.1051/matecconf/202032602002.
[24] D.T.L. Alexander, A.L. Greer, "Solid-state intermetallic phase tranformations in 3XXX aluminium alloys", *Acta Mater.*, vol. 50, no. 10, pp. 2571–2583, 2002, https://doi.org/10.1016/S1359-6454(02)00085-X.
[25] D.T.L. Alexander, A.L. Greer, "Nucleation of the Al6(Fe, Mn)-to-α-Al-(Fe, Mn)-Si transformation in 3XXX aluminium alloys. I. Roll-bonded diffusion couples", *Philos. Mag.*, vol. 84, no. 28, pp. 3051–3070, 2004, https://doi.org/10.1080/14786430410001701760.
[26] Y. Liu, L. Luo, C. Han, L. Ou, J. Wang, C. Liu, "Effect of Fe, Si and Cooling Rate on the Formation of Fe- and Mn-rich Intermetallics in Al-5Mg-0.8Mn Alloy", *J. Mater. Sci. Technol.*, vol. 32, no. 4, pp. 305–312, 2016, https://doi.org/10.1016/j.jmst.2015.10.010.
[27] Y.J. Li, L. Arnberg, "A eutectoid phase transformation for the primary intermetallic particle from Alm(Fe,Mn) to Al3(Fe,Mn) in AA5182 alloy", *Acta Mater.*, vol. 52, p.2945–2952, 2004. https://doi.org/10.1016/j.actamat.2004.02.041.
[28] Y. Du, Y.A. Chang, B. Huang, W. Gong, Z. Jin, H. Xu, Z. Yuan, Y. Liu, Y. He, F.Y. Xie, "Diffusion coefficients of some solutes in fcc and liquid Al: Critical evaluation and correlation", *Mater. Sci. Eng. A*, vol. 363, no. 1–2, pp. 140–151, 2003, https://doi.org/10.1016/S0921-5093(03)00624-5.
[29] K.E. Knipling, D.C. Dunand, D.N. Seidman, "Criteria for developing castable, creep-resistant aluminum-based alloys - A review", *Int. J. Mater. Res.*, vol. 97, no. 3, pp. 246–265, 2006, https://doi.org/10.3139/146.101249.
[30] R. Goswami, G. Spanos, P.S. Pao, R.L. Holtz, "Precipitation behavior of the β phase in Al-5083", *Mater. Sci. Eng. A*, vol. 527, no. 4–5, pp. 1089–1095, 2010, https://doi.org/10.1016/j.msea.2009.10.007.
[31] S. Lee, S. Wu, "Identification of Dispersoids in Al-Mg Alloys Containing Mn", *Metallu. Trans. A*, vol. 18, no. August, pp. 1353–1357, 1987.
[32] X.L. Xiao, H.W. Liu, W.L. Chen, Y.M. Lin, "Morphology of Dispersoids in an Annealed Al-Mg Alloys", *Mater. Sci. Forum*, vol. 1035, p.72–82, 2021. https://doi.org/10.4028/www.scientific.net/msf.1035.72.
[33] Y.J. Li, L. Arnberg, "Solidification structures and phase selection of iron-bearing eutectic particles in a DC-cast AA5182 alloy", *Acta Mater.*, vol. 52, no. 9, pp. 2673–2681, 2004, https://doi.org/10.1016/j.actamat.2004.02.015.
[34] J. Osten, B. Milkereit, C. Schick, O. Kessler, "Dissolution and precipitation behaviour during continuous heating of Al-Mg-Si alloys in a wide range of heating rates", *Materials (Basel).*, vol. 8, no. 5, pp. 2830–2848, 2015, https://doi.org/10.3390/ma8052830.
[35] E. Romhanji, T. Radeti, M. Popovi, "Homogenization of an Al-Mg alloy and alligatoring failure alloy ductility and fructure", Mater. Tehnol., vol. 50, no. 3, pp. 403–407, 2016, https://doi.org/10.17222/mit.2015.110.

[36] E. Romhanji, T. Radetić, M. Popović, "Homogenization of an Al-Mg alloy and alligatoring failure: Influence of the microstructure", Mater. Tehnol., vol. 50, no. 4, pp. 531–536, 2016, https://doi.org/10.17222/mit.2015.111.